PHOTOELECTRONS AND SOLAR WIND/LUNAR LIMB INTERACTION*

DAVID R. CRISWELL
*The Lunar Science Institute**, Houston, Tex., U.S.A.*

(Received 16 November, 1972)

Abstract. It is suggested that boundary conditions for solar wind/lunar limb interactions are active. The 'whole-Moon' limb does not evoke a shock cone because warm ($\simeq 13$ eV/electron) solar wind electrons are replaced by cool ($\lesssim 2$ eV/electron) photoelectrons that are ejected from the generally smooth areas of the lunar terminator illuminated at glazing angles by the Sun. A localized volume of low thermal pressure is created in the solar wind by these cool photoelectrons. The solar wind expands into this turbulence-suppressive volume without shock production. Conversely, directly illuminated highland areas exchange hot photoelectrons (>20 eV/electron) for warm solar wind electrons. The hot electrons generate a localized pressure increase (Δp) in the adjacent solar wind flow which evokes a shock streamer in the solar wind. Shock streamers are identifiable by a coincident increase in the magnitude ($\Delta B \sim \Delta p$) of the solar wind magnetic field immediately external to the lunar wake. Shock occurrence is controlled by lunar topography, solar activity in the hard ultraviolet (>20 eV), solar wind electron density and thermal velocity, and the intensity of the solar wind magnetic field.

1. Introduction

Observations by Colburn *et al.* (1967), Ness *et al.* (1967), and Lyon *et al.* (1967) of the wake structure evoked in the solar wind downstream of the Moon pose a definite problem (Figure 1). The Moon is immersed in a solar wind flow which is always supersonic. Thus, in analogy with the Earth, a definite shock structure should exist downstream. Such a shock would be characterized by local increases of plasma density (ϱ), pressure (p) and the magnitude B_{sw} of the solar wind magnetic field $\mathbf{B}_{sw}$. However, a shock is usually not observed at the distances of 2–5 R_m ($R_m = 1738$ km $\sim$ lunar radius) from the Moon accessible to the lunar orbiting Explorer 35. Rather, a region devoid of plasma is produced (region 2). The solar wind plasma simply expands into this downstream void until a pressure balance ($p + B_{sw}^2/8\pi = B_v^2/8\pi$) is achieved between the enhanced magnetic field (B_v) of the void region and the total external solar wind pressure. The Moon as a whole evokes a gentle, nearly undisturbed flow pattern in the solar wind rather than a shock. The void/solar wind boundary (1) is usually characterized by a locally decreased magnetic intensity ($-\Delta B$). Electron surface currents in the boundary induce this diamagnetic decrease.

The problem became a dilemma when subsequent observations were made of shock streamers (Ness *et al.*, 1968; Colburn *et al.*, 1971) external to the wake (point 3 in Figure 1). The streamers are generated when specific lunar highland features are present on or near the lunar terminator. The basic problem is clear: Why do specific

* Paper dedicated to Professor Harold C. Urey on the occasion of his 80th birthday on 29 April 1973.
** The Lunar Science Institute is operated by the Universities Space Research Association under Contract No. NSR 09-051-001 with the National Aeronautics and Space Administration.

The Moon 7 (1973) 202–238.

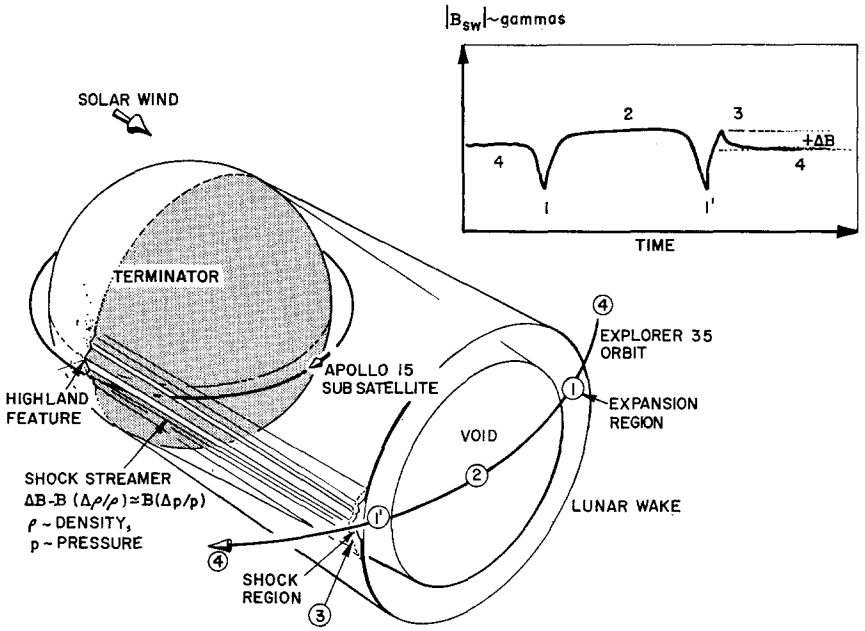

Fig. 1. Four significant features of the plasma flow downstream of the Moon are illustrated. Region (2) is devoid of solar wind plasma due to accretion and neutralization of ions and electrons on the sunward hemisphere. Region (4) is the undisturbed solar wind. Considerable theoretical work has been directed toward explaining the morphology of the expansion region (4) in terms of either magnetohydrodynamic flow or of free streaming particles. The highland associated shock streamer (region (3)) is not consistent with these theories. Generally similar downstream magnetic profiles are measured by the high altitude Explorer 35 and the low altitude ($\simeq$100 km) Apollo-15 subsatellite.

small scale (10–100 km) lunar regions, when located in or near the terminator, evoke shock streamers while the entire lunar limb ($\simeq$10900 km) does not?

Separate approaches have been suggested in the literature to explain the lack of an overall lunar shock and the sporadic occurrence of shock streamers. Lack of a 'whole-Moon shock' is credited to the complete adsorption and electrical neutralization by the lunar surface of solar wind plasma striking the sunward hemisphere (Gold, 1966; Sonett and Colburn, 1967, 1968; Johnson and Midgley, 1968). Siscoe *et al.* (1969) and Spreiter *et al.* (1970) have noted that the neutralizing and adsorptive ability of the Moon must be extremely precise to produce no more deviation of the wake plasma than observed. In addition, the low internal electrical conductivity of the lunar bulk ($\lesssim 10^{-5}$ mhos cm^{-1}) permits the solar wind magnetic field to convect unhampered through the Moon. Thus, no significant magnetic field increases occur in front of or inside the sunward hemisphere which could couple into the adjacent solar wind flow and evoke a general shock (Sonett *et al.*, 1972). Dryer (1968) pointed out that the lack of a lunar bow shock at 1.5 R_m precluded flow coupling of the Moon and solar wind on the scale of the cyclotron radius ($r_p \simeq 100$ km) corresponding to the thermal velocity of solar wind protons.

Recent observations indicate these contentions of *minimal interaction* are not completely true. Anderson *et al.* (1972) analyzed the flux of the higher energy solar wind electrons (>500 eV) encountered at low altitudes ($\simeq 100$ km) by the Apollo-15 lunar orbiting subsatellite. They detected enhanced fluxes at approximately 60° off the Sun–Moon line which appear to define a region of turbulence. Location of the electron turbulence region does not appear to be influenced by lunar features. Neugebauer *et al.* (1971), report that the energy of keV-ions striking the sunlit surface is suppressed from their energy in the free flowing solar wind due to the presence of local magnetic fields. Freeman (1972) and Snyder *et al.* (1970) report the detection of solar wind ions prior to local sunrise, just after local sunset, and deep into local lunar night when the Moon is immersed in the solar wind. Pre-sunrise and post-sunset detection of electrons and rapidly time varying electron fluxes are also reported (Clay *et al.*, 1972; O'Brien *et al.*, 1971). These observations indicate that the Moon does interact with the solar wind at least up to distances of 100 km from the surface and bring into questioning the 'perfect adsorption and neutralization' conditions utilized in previous theoretical models of lunar/solar wind interaction.

Theoretical explanations of the localized limb shocks or shock streamers assume that either induced, or more likely, remanent magnetic fields about certain lunar highlands couple with the solar wind plasma. A volume of higher pressure ($p+\Delta p$) is generated in the adjacent flow which slightly deflects the solar wind and produces a weak shock characterized by the increased solar wind magnetic field strength (Barnes *et al.*, 1971; Mihalov *et al.*, 1971; Hollweg, 1968, 1970; Schwartz *et al.*, 1969; Whang and Ness, 1970).

Figure 2 is a composite of data from Coleman *et al.* (1972) and Sonett and Mihalov (1972) displayed on an outline map of the lunar surface between 60° N and 60° S lat. Underlined numbers in the fine-lined grids (15° by 15°) indicate the fraction of wake crossings by the Explorer-35 during which shock streamers were detected. These fractions are significant to more than one standard deviation (i.e., the ratio of shock streamer observations to total scans in a given 15° by 15° grid element differs from the mean ratio over all observations by more than 1σ). The Levi Civita grid (140° E, 20° S) has $\sigma \simeq 6.3$. There is a statistically significant lack ($\sigma < -1$) of detectable shock streamers for latitudes poleward of 30° N and 30° S based on 30 observations. Astrices indicate grids in which $\sigma < -1$. Grids with no numbers have $-1 < \sigma < +1$.

There is a clear overlap between the source regions of the shock streamers and the lunar terrae (used in place of 'highlands' by Kaula *et al.* (1972)) to denote rough areas which do not necessarily have the largest selenocentric extent). Refer to composite maps of the lunar surface and source locations presented by Mihalov *et al.* (1971) for graphic displays of this association.

Dashed grids identify shock source regions detected fron the Apollo-15 subsatellite. Numbers in parentheses indicate the fraction of terminator crossings during which shock-like effects were observed as based on preliminary quick-look data (Coleman *et al.*, 1972). Comparison of the overlapping data is interesting. Near the strong shock-source region (30° S, 175° W) both the low altitude ($\simeq 100$ km) subsatellite and

the high altitude (1.5–5R_m) Explorer-35 observed shock effects. Likewise, there are several regions (30° S, 30° W), (20° N, 10° E), and (20° N, 170° E) where neither satellite detected shocks. However, agreement is not complete. Notice (30° S, 140° W), (30° S, 50° W), (30° S, 0° W), and (20° N, 90–150° E) where the subsatellite does observe shock-effects and Explorer-35 does not. This inconsistency reveals that Moon/solar-wind interactions occur which do not evoke fully developed shock streamers.

Conversely, grid elements (20° N, 165° W) and (20° N, 160° E) are interesting for the opposite effect. Explorer-35 observed shocks from these regions whereas the subsatellite did not. If a local remanent magnetic field (magcon), which must be constant in scale size and strength over geologic time, is the *sole* agent inducing shocks then the subsatellite should always observe terminator interactions in the source region as located by means of Explorer-35 data. Negative correlation for these three grid elements strongly supports the contention that *other* processes, possibly of solar wind and/or solar photon origins, also affect or control the shock-production process. One other aspect of this joint analysis supports the multi-factor contention. Shock effects were observed on every low altitude overflight of grid (30° S, 175° W) whereas Explorer-35 observed shocks only 40% of the time. Grids (20° S, 140° E) and (10° S, 170° E), the most effective source regions of Explorer-35 shocks, had production rates of the order of 0.6. Multiple factors must be operating which damp or reduce shock streamer development between 100 km altitude and 1.5–5 R_m.

Also shown are contours proportioned to the absolute value of the local component of lunar magnetism (B_T) roughly coplaner with the ecliptic plane. Refer to Coleman *et al.* (1972) for details of the analysis. B_T is adjusted to an altitude of 93 km by the observationally justified relation $B(93\text{ km}) = B(h)$. $(93\text{ km/h})^{2.5}$ where B_T (Van De Graaff) $= 0$ was chosen as the reference point because the field change ($\Delta B_T \simeq 1\gamma$) was greatest over that crater (25° S, 175° E). Vector **B** (Van De Graaff) is inward directed. *In this representation the total field intensity decreases as the numerical value of B_T increases.* Several relations of the B_T-contours and the Explorer-35 grid are interesting.

Adjacent grids (20° S, 175° E) and (20° S, 160° E) produce shocks 40% of the time, however, $B_T \simeq 26$–30 is overall much larger in the 160° E grid than in the 175° E grid ($B_T \simeq 0$–36). Complete B_T measurements in the Levi Civita grid (20° S, 140° E) and (10° S, 170° E) grid will be very interesting. There is no obvious correlation between the shock occurrence rate (SF) at high altitudes and B_T as one scans the B_T-contours. At grid (10° S, 160° W) SF = 0.3 and $B_T \simeq 30$–44. Whereas, at grid (10° N, 130° W) $B_T \simeq 22$–40 there is a statistically significant lack of shocks ($\simeq -1.1\sigma$); the maria grid (20° N, 20° W) with $B_T \simeq 28$–30 has a -1.3σ lack of shock activity; and the Hecataeus grid (20° S, 80° E) has $B_T \simeq 30$–36 with a statistically insignificant shock occurrence fraction.

Whang and Ness (1972) contend there is not a correlation of limb shock occurrence with the location of specific lunar features on the terminator and indirectly maintain that one is observing whole-Moon shocks rather than shock streamers. They organized the shock occurrence data in terms of latitude strips rather than a latitude-longitude grid system. Their contention is not tentable in view of the subsatellite observations of selenographically controlled shock production.

Sonett and Mihalov (1972) show for $\Delta B > 0.7\gamma$ that there is not an obvious dependence of ΔB with downstream distance from the terminator. However, the ratio LPI/SPI increases and then decreases with increasing downstream distance where SPI indicates 'small positive enhancements' defined as $0 < \Delta B/B_{sw} < 0.1$ and $\Delta B/B_{sw} \gtrsim 0.1$ are termed 'large positive increases' or LPI's (Whang and Ness, 1972). These data indicate that the Moon produces large shocks which extend unabated 5 R_m or more downstream. However, a mid range of shocks (LPI) are also produced that damp-out inside of 5 R_m and the damping displays some sensitivity to the thermal energy density of the solar wind.

Comparison of shock activity based on the high altitude Explorer-35 observations, preliminary data from the low altitude subsatellite, and Alsep observations of the solar wind indicate the following: (1) Complete adsorption and neutralization of solar wind plasma on the sunward lunar surface does not explain the lack of a whole-Moon shock; (2) deflections and turbulence of solar wind plasma occurs near the terminators which means that smooth flow of solar wind past the lunar limb does not always occur; (3) extensive surface magnetic fields (magcons) do not provide a unique explanation for production of shock streamers – other factors must be important; and (4) shock-like activity near the Moon does not necessarily evoke strong shock streamers downstream along the wake possibly because of solar wind conditions.

The basic concept in this paper is that the Moon/solar wind boundary conditions are active rather than passive. There is significant flow of energy between the lunar surface and the solar wind which results from the interchange of solar wind electrons with lunar photoelectrons. Lack of a 'whole-Moon' shock is due to the replacement of *warm* solar wind electrons ($\simeq 13$ eV/electron) by *cool* photoelectrons ($\lesssim 2$ eV/electron) ejected from the generally smooth areas of the Moon which are illuminated at glazing angles by the Sun. These cool photoelectrons provide an energy sink for turbulence generated as the solar wind flows past the Moon. Highland areas emit hot photoelectrons ($\gtrsim 20$ eV/electron) due to the direct exposure of highlands to the solar flux. Warm solar wind electrons are replaced by hot photoelectrons which generate a high pressure region in the solar wind and thus evoke weak shocks. Static magnetic fields of a lunar origin (magcons) have a secondary role in this model and provide a secondary source of magnetic pressure ($B^2_{Moon}/8\pi$) for shock generation. A simple model of the exchange process is presented in the following section. Subsequently, detailed analyses of each feature of the model are presented.

2. Simple Exchange Model

The excess pressure required to deflect the solar wind flow outward from the void region and produce a shock streamer is related to the bulk flow of the protons as defined in Equation (1). Shock angles (θ) or deflections of 3° to 7° are observed and are theoretically consistent with the observed ΔB and ΔQ increases (Sonett and Mihalov, 1972; Siscoe *et al.*, 1969)

$$\Delta Q = MNV^2 \sin^2\theta \simeq 0.37 \text{ to } 1.6 \times 10^{-10} \text{ dynes cm}^{-2} \quad (1)$$

or

$\Delta\eta \simeq 23$–100 eV cm^{-3} (thermal energy equivalent of excess electron pressure)

where $M \sim$ proton mass, $N \sim$ proton number density ($\simeq 5$ cm^{-3}), $V \sim$ solar wind bulk velocity ($\simeq 400$ km s^{-1}), $\theta \sim$ deflection angle of the shock streamer ($\simeq 3$ to $7°$), and $\Delta\eta$ is the *excess thermal energy density* of the electrons in the coupling region.

Figure 3 illustrates the exchange of solar wind electrons and photoelectrons over adjacent highland and maria features. Solar photon and solar wind proton flows are assumed to be along the antisolar direction and approximately perpendicular to the lunar radius vector at the terminator. Highland faces fully intercept both fluxes. Photon and proton fluxes to the surrounding flat terrain are decreased by the factor $\cos(\alpha)$ which is approximately 10^{-2} in the terminator zone. In contrast the net solar wind electron flux (i.e., electron flux minus proton flux) is approximately omnidirectional and the same to unit areas on the highlands and flat lands. The extreme thermal motion of the solar wind electrons produces the omnidirectional electron flux (Hundhausen, 1970). Charge neutrality in the solar wind demands the thermal electron flux (F_{sw}) to either a highland or flatland area be exactly balanced by an equal flux ($F(\varepsilon_b)$) of photoelectrons ejected from that local surface area. This balance must occur in less than the scale of the solar wind Debye length ($\lambda_D \simeq 10^3$ cm). That is, charge neutrality applies over scales greater than 10^3 cm. The radii of the stream tubes are indicative of the cyclotron radii of electrons which dominate the local particle population. As explained in the following section, the highland photoelectrons will be more energetic and tend to have larger cyclotron radii. The converse is true for the flatland

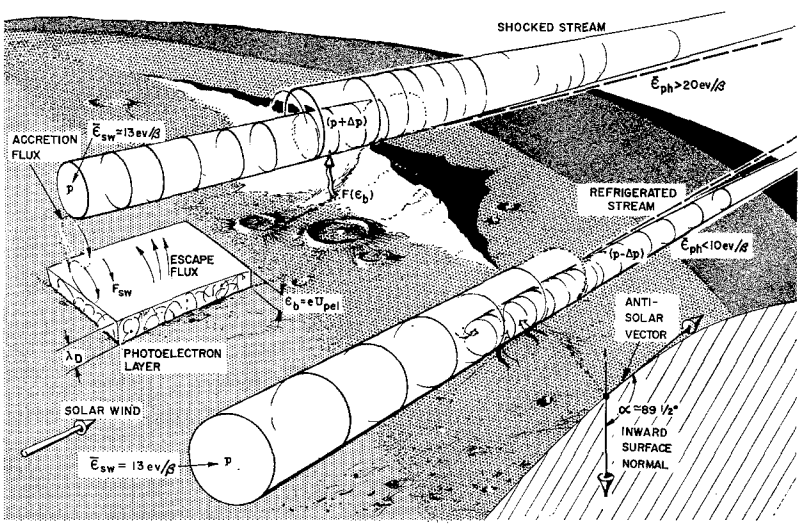

Fig. 3. The terminator exchange of warm solar wind electrons for hot photoelectrons above a highland feature (top streamline) or cool electrons above a flatland region (lower streamline) is depicted. It is assumed that V and B_{sw} are parallel.

electrons. The number of rings along each flux tube is indicative of the number density of solar wind electrons (upstream) or photoelectrons (confluence region) at that point. The exchange occurs along several kilometers of streaming distance and over a vertical distance of one to two electron cyclotron radii (0.5–5 km). Surface electric fields (U_{pel}) will be shielded from the solar wind by the layer of low energy photoelectrons which extends only a few tens of meters above the surface. U_{pel} will adjust to insure balance of accreting solar wind electrons and escaping photoelectrons. Turbulence will occur in the downstream flow as the new electrons readjust their spatial distribution so as to insure change neutrality over elements approximately $(\lambda_D)^3$ in volume. B_{sw} is usually not parallel to V. Problems of the non-parallel situation are discussed in the final section.

Even though numerical flux balance ($F(\varepsilon_b) = F_{sw}$) must occur there is not necessarily a balance of energy fluxes. The average thermal energy of a solar wind electron is 13 eV. The corresponding *electron thermal energy density* (η) is 65 eV cm^{-3}. A *total thermal electron energy density* (η_T) the order of 88 to 165 eV cm^{-3} must be present in the coupling region to produce the shock streamer (Equation (2))

$$\eta_T = \eta + \Delta\eta. \tag{2}$$

Equation (2) assumes there is no change in the thermal energy density of the protons in the interchange region.

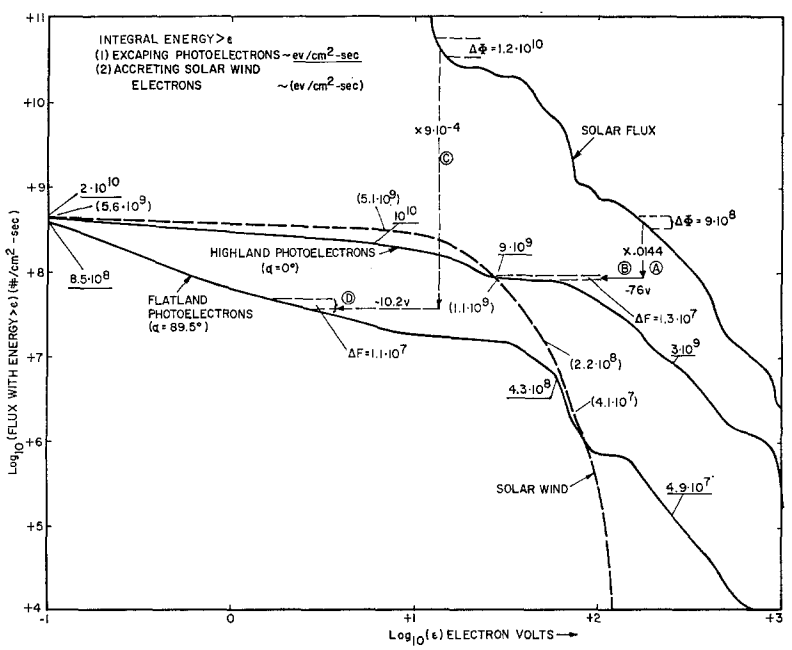

Fig. 4. Displayed are log-log curves of the integral flux of solar photons or electrons with energy greater than ε incident on or exiting surfaces on the lunar terminator versus ε. Refer to the text for details of this simple model.

Figure 4 is the quantative summary of a simple production model for photoelectrons. The abscissa is the log to the base 10 of photon or electron energy in electron volts. The ordinate is the log to the base 10 of the *integral* flux of photons ($\phi(>\varepsilon)$) or electrons ($F(>\varepsilon)$), as the case may be, with energies greater than a given energy ε. The 'Solar Wind' curve specifies the solar wind electron flux to a surface of arbitrary orientation. A Maxwellian velocity distribution characterized by $\frac{3}{2}$ kT = 13 eV and 5 electrons cm^{-3} is assumed. The total electron flux is approximately 4.3×10^8 electrons cm^{-2} s^{-1} which correspond to average solar wind conditions (detailed in following section). The 'Solar Flux' curve is the integral photon flux perpendicular to the Sun/Moon line for a period of moderate (non-flare solar) activity (Hinteregger, 1970; Johnson, 1961; Wende, 1972; Walbridge, 1970).

Photoelectron production from an illuminated highland is calculated by assuming that 10% of the solar photons of energy $h\nu$ evoke a spectrum of photoelectrons ranging from $h\nu$ to 0 eV in energy with approximately 10% of these photoelectrons having en energy within 10% of $h\nu$. Photoelectron production in the surface is approximately equivalent to reducing the 'Solar Flux' curve by 10^{-2}. Note line A, $\Delta\Phi$, and ΔF in Figure 4. However, a photoelectron produced in the surface must pass through the surface 'work function' (w) to escape the material and will lose approximately 5 eV of energy. In addition, to enter the solar wind a photoelectron must pass through the surface cloud of lower energy photoelectrons. These lower energy photoelectrons are momentarily in ballastic trajectories above the surface material. An electric field is created between these electrons and their balancing positive surface charge which returns these low energy electrons to the surface. The total electrical potential drop of U_{pel} will be present across the cloud. For this case the total energy reduction is $eU_{pel} = 76$ eV which is subtracted from the reduced 'Solar Flux' curve shifting it to the left to produce the 'Highland Escape Curve' (note line B). 'U_{pel}' is equal to the photoelectron energy at the surface for which the integral flux of more energetic photoelectrons ($F(\varepsilon' > \varepsilon_b = eU_{pel})$) equals the accreting solar wind flux ($F_{sw}(>0$ eV)).

Numbers along the escape and solar wind curves indicate the total energy in eV cm^{-2} s^{-1} conveyed by the respective electrons of energy greater than that indicated by the abscissa value of the arrows. Solar wind electrons deposit approximately 5.6×10^9 eV cm^{-2} s^{-1} whereas the escaping energy flux is approximately $3\frac{1}{2}$ times larger at 2×10^{10} eV cm^{-2} s^{-1}. Warm solar wind electrons are replaced by hot photoelectrons. This photoelectron energy flux is sufficient to generate 7° shock streamers.

Significantly, photons of $\varepsilon_0 > 82$ eV, that is 150 Å or less in wavelength, contribute more than 50% of the escape energy. The presence of shock streamers should correlate with increased solar output in the extreme UV and soft X-ray regions. Kreplin (1970) notes that the 44–60 Å solar output may vary by 2 to 5 over short times and a factor of 20 over a solar cycle while the 8–20 Å band displays corresponding long term variations of 200 in intensity.

Consider next adjacent flat terrain which is illuminated by a setting Sun ($\alpha = 89.5°$). The solar wind electron flux per unit area is essentially the same as the highland case. However, the 'Solar Flux' curve must be decreased by cos $89.5° = 8.7 \times 10^{-3}$ or more

due to the approach of sunset. The solar diameter is approximately 0.5°. The previous corrections for yield and energy loss also apply and the 'flatlands escape' curve results. The escaping energy flux of 8.5×10^8 eV cm^{-2} s^{-1} is 0.15 of the input energy flux. The 'warm' solar wind electrons are replaced by 'cool' photoelectrons. No shock is produced in the solar wind since there is no local overpressure. In fact, a slight pressure decrease results which should smooth the solar wind flow and provide a sink for energy generated by plasma turbulence at the limb.

The reduction factor for the flatlands (note line C) is not equal to $(0.2)(0.1)(\cos 89.50) = 1.7 \times 10^{-4}$ due to contributions of higher energy photons to the energy interval at the end of line D and to the action of the surface electric field. Equation 12 with $p = 25$, $q = 0$, $w = 5$ V, and $\varepsilon_p = 0.9\ \varepsilon_0$ was used to produce these curves.

This introduces the basic physical processes and general experimental observations which motivate consideration of the model of photoelectron exchange with solar wind electrons as the critical factor in solar wind/Moon interactions. In the following sections detailed considerations are given to the range of excess pressure required for shock production, variations of the energy input by solar wind electrons, and detailed models for photoelectron production. Characteristics of the shock region and the role of solar wind heat conduction in the suppression of poleward shocks will be qualitatively discussed. Additionally, the role of lunar topography in the production of limb shocks will be discussed. Refer to Criswell (1973) for an alternative illustration of the process.

3. Modeling Considerations

A. SHOCK PRESSURE

The excess pressure required to produce a shock can be calculated from Equation (1). The shock angle (θ) is a function of the solar wind parameters V, B_{sw}, and N. To first order $\theta = \arctan (V_A/V)$ where $V_A = (B_{sw}/(4\pi NM))$ is the local Alfvén velocity. For small values $\tan\theta \simeq \theta$(radians), which combined with Equation (1) yields

$$\begin{aligned} \Delta\eta &= \Delta p/(1.6 \times 10^{-12}\ \text{erg eV}^{-1}) = \\ &= \left(\frac{M}{1.6 \times 10^{-12}}\right)(NV^2)\,(B_{sw}^2/V^2 4\pi NM) = \\ &= B_{sw}^2/(4\pi)\,(1.6 \times 10^{-12}) \simeq 5\,(B_{sw}(\text{gammas}))^2\ \text{eV cm}^{-3}. \end{aligned} \tag{3}$$

Ness *et al.* (1971) observed $\bar{B}_{sw}(< 300\ \text{km s}^{-1}) \simeq 3\gamma$ which corresponds to quiet conditions with $T_p < 2 \times 10^4$ K, while $\bar{B}_{sw}(\text{avg}) \simeq 5\gamma$ all other conditions with $B_{sw}(\text{min}) \simeq 1.7\gamma$ and $B_{sw}(\text{max}) \simeq 8\gamma$, where $T_p \sim$ solar wind proton temperature.

Thus:

$$\Delta\eta\,(\text{eV cm}^{-3}) = \begin{array}{l} 14\ (\text{very quiet},\ T_p < 2 \times 10^4\,\text{K}) \sim B_{sw}(\text{minimum}) \\ 45\ (\text{quiet},\ T_p < 2 \times 10^4\,\text{K}) \sim \bar{B}_{sw} \\ 125\ (T_p > 2 \times 10^4\,\text{K},\ \text{avg. and fast}) \sim \bar{B}_{sw} \\ 245\ (\text{fast} - \text{disturbed}) \sim B_{sw}(\text{max}) \\ 320\ (\text{average}) \sim B_{sw}(\text{maximum}) \end{array}$$

TABLE I

Solar wind description		Data $N(\beta\,\mathrm{cm}^{-3})$	ε_{sw}(eV)	$v_t(\mathrm{cm\ s}^{-1}) \times 10^8$	Derived conditions B_{sw} (gamma)	$F_{sw}(\mathrm{cm\ s}^{-1}) \times 10^8$	$E_{sw}(\mathrm{eV\ cm}^{-1}\,\mathrm{s}^{-1}) \times 10^9$ balance	shock	$\varepsilon_s(\mathrm{eV}/\beta)$
		(1)	(2)	(3)	(4)	(5)	(6)	(7)	(8)
1. Very Quiet	(a)	4	6	1.3	1.8[a]	1.5	0.9	1.4	9.5
$T_p < 2 \times 10^4$K	(b)	4	6	1.3	$\overline{3}$[b]	1.5	0.9	2.6	$\overline{17}$[b]
$V(\mathrm{km\ s}^{-1}) < 300$	(c)	4	6	1.3	5	1.5	0.9	6.6	44
2. Quiet	(a)	20	13	2	2.5	11	14	17	15
$T_p > 2 \times 10^4$K	(b)	20	13	2	$\overline{5}$	11	14	2121	$\overline{19}$
$300 < V(\mathrm{km\ s}^{-1}) < 400$	(c)	20	13	2	6.8	11	14	28	25
3. Average	(a)	7.7	13	2	2.5	4.3	5.6	7.3	17
$400 < V(\mathrm{km\ s}^{-1})$	(b)	7.7	13	2	$\overline{5}$	4.3	5.6	12	$\overline{29}$
< 550	(c)	7.7	13	2	8.3	4.3	5.6	25	58
4. Fast-	(a)	2	17[a]	2.3	3.7	1.3	2.2	6.1	47
disturbed	(b)	2	17	2.3	$\overline{5}$	1.3	2.2	10	$\overline{80}$
$V(\mathrm{km\ s}^{-1}) > 550$	(c)	2	17	2.3	6.8	1.3	2.2	18	140

[a]Used for extremal estimates
[b]Appropriate to the average values for this solar wind flow
β – Electron

Table I presents the ranges of proton density (N) and average solar wind electron energy (ε_{sw}) [or thermal velocity v_t] based on discussions by Serbu (1972) and Hundhausen *et al.* (1970). A systematic dependence of electron temperature (i.e., ε_{sw}) on proton temperature (T_p) has *not* been experimentally observed. The ε_{sw} arrangement is simply to allow extremal values of ε_s to be determined. 'ε_s' is the average energy each escaping photoelectron must convey into the solar wind in order to produce a shock.

The total electron energy required to evoke a shock is given by

$$\varepsilon_s = (\Delta\eta + \eta)/N. \tag{4}$$

B. SOLAR WIND ELECTRON FLUX

Energetic photoelectrons will escape into the solar wind to replace accreting solar wind electrons (F_{sw}). Flux balance ($F_{sw} = F(>\varepsilon_b)$ will occur at some photoelectron energy ε_b. Photoelectrons with total energy $\varepsilon < \varepsilon_b$ will be returned to the lunar surface. Equation (5) (Grobman and Black, 1969) specifies the solar wind electron flux (F_{sw}) to the sunlit lunar surface as a function of solar wind electron density (n), electron thermal velocity (v_t), the angle between an inward directed surface normal and the Sun–Moon line (α), and $u \equiv V/v_t$

$$F_{sw} = \frac{nv_t}{2\pi^{1/2}} \{\exp(-u^2 \cos^2\alpha) + \pi^{1/2} u \cos\alpha [1 + \operatorname{erf}(u \cos\alpha)]\}. \tag{5}$$

Two cases are of interest in this discussion of terminator accretion. Net flow to a highland face corresponds to $\alpha = 0°$ where the proton flux is subtracted and net flow to a flat region corresponds to $\alpha \approx 90°$ where the proton flux is negligible.

$$F_{sw}(\text{flat region}) = nv_t/2\pi^{1/2}, \tag{6}$$

$$F_{sw}(\text{mountain}) = \frac{nv_t}{2\pi^{1/2}} [\exp(-u^2) + \pi^{1/2} u (1 + \operatorname{erf} u)] - NV$$

$$\simeq F_{sw}(\text{flat region}) \times$$

$$\times \left\{\exp(-u^2) + \pi^{1/2} u (1 + \operatorname{erf} u) - 2\pi^{1/2} \frac{NV}{nv_t}\right\}. \tag{7}$$

Physical conditions of the solar wind were summarized in Table I. The electron thermal velocity (Table I) as observed to date appears to be statistically independent of solar wind proton conditions. The average electron temperature is $1.5 \times 10^{+5}$ K and varies between 0.67 and $2 \times 10^{+5}$ K. This corresponds to a thermal velocity (v_t) range 1.3×10^3 km s$^{-1} < v_t < 2.3 \times 10^{+3}$ km s^{-1} and average thermal velocity $v_t \simeq 2 \times 10^3$ km s^{-1}. Phenomenologically the electron flux to the flat regions (Equation (6)) is most dependent on the electron number density. Charge neutrality requires the electron and proton densities to be equal except for a 10% or less correction due to the presence of completely ionized helium. Proton density (N) can be used to approximate n (i.e., $N \simeq n$).

The extreme values and range of average values of solar wind electron flux (F_{sw}) and the corresponding electron thermal energy input rate (E_{sw}) to the flatlands are given in Table I by columns (5) and (6).

The solar electron flux to the highlands (F_{sw}) is specified by Equation (17). If one assumes $N/n \simeq 1$ then the variation of $u = V/v_t$ is the remaining significant factor. The observed range of V is 290 (very quiet) $< V$ (km sec^{-1}) < 550 (very disturbed) with V (average) $\simeq 400$ km sec^{-1} (Hundhausen *et al.*, 1970). Utilizing the extreme values of u_t we have

$$u = \begin{cases} 5.5 \times 10^7/1.3 \quad \times 10^8 = 0.41 \text{ (maximum)} \\ 4 \times 10^7/2 \quad \times 10^8 = 0.2 \text{ (average)} \\ 2.9 \times 10^{+7}/2.3 \times 10^8 = 0.126 \text{ (minimum).} \end{cases} \tag{8}$$

Define $\Delta F = \exp(-u^2) + \pi^{1/2} u (1 + \operatorname{erf} u) - 2\pi^{1/2} u$. The values $\Delta F(u \sim \max) = 0.956$, $\Delta F(u \sim \text{average}) = 0.981$, and $\Delta F(u \sim \text{minimum}) = 0.903$ demonstrate the reasonable insensitivity of ΔF to the maximum possible range of u. N and v_t are, therefore, the significant physical parameters controlling the net electron flux to the highlands and the flatlands. The extreme values of F_{sw} in Table I will be used to determine the values of ε_b (minimum energy of escaping photoelectrons) for various solar wind conditions by determining the value of photoelectron energy $\varepsilon = \varepsilon_b > \varepsilon_{ph}$ which $F(\varepsilon > \varepsilon_{ph}) = F_{sw}$.

C. PHOTOELECTRON PRODUCTION

The model for photoelectron production used to illustrate the exchange process is too simple for realistic calculations and a parametric analyses. Equation (9) is the analytical expression for the surface production rate of photoelectrons of energies ε' to $\varepsilon' + d\varepsilon'$ by photons of energy ε_0 of the form

$$f(\varepsilon') = \frac{G \cos \alpha}{2} Y(\varepsilon_0)\, \varrho(\varepsilon'/\varepsilon_0)\, \varphi(\varepsilon_0), \tag{9}$$

$\sim$ photoelectrons cm^{-2} s^{-1} sterad^{-1} eV^{-1} where $Y(\varepsilon_0) \sim$ total number of electrons emitted per incident photon of energy ε_0; $\varphi(\varepsilon_0) \sim$ # photons cm^{-2} s^{-1} eV^{-1} at the energy ε_0; $\varrho(\varepsilon'/\varepsilon_0) \sim$ energy distribution of emitted photoelectrons with $\int_0^{\varepsilon_0} \varrho(\varepsilon'/\varepsilon_0)\, d\varepsilon' = 1$; and G is the solid angle through which photoelectrons can escape. Isotropic emission of photoelectrons over the outward hemisphere is assumed. All solar photons with $\varepsilon_0 > \varepsilon'$ contribute to production of the ε'-energy distribution

$$\frac{dF(\varepsilon')}{d\varepsilon'} = \int_{\varepsilon_0 = \varepsilon'}^{\infty} f(\varepsilon' < \varepsilon_0)\, d\varepsilon_0, \tag{10}$$

and to the *integral flux* of photoelectrons with energies greater than ε of

$$F(>\varepsilon) = \int_{\varepsilon'=\varepsilon}^{\infty} (\mathrm{d}F(\varepsilon')/\mathrm{d}\varepsilon')\,\mathrm{d}\varepsilon' =$$

$$= \int_{\varepsilon'=\varepsilon}^{\infty} \int_{\varepsilon_0=\varepsilon'}^{\infty} G \frac{\cos\alpha}{2\pi} Y(\varepsilon_0)\, \varrho(\varepsilon'/\varepsilon_0)\, \Phi_0(\varepsilon_0)\,\mathrm{d}\varepsilon'\,\mathrm{d}\varepsilon_0 . \qquad (11)$$

Calculations of the photoelectron production will be based on the following approximation of $\varrho(\varepsilon'/\varepsilon_0)$ which is the differential energy distribution function for the photoelectron evoked by photons of energy ε_0.

$$\varrho(\varepsilon'/\varepsilon_0) = B \cdot \begin{cases} 0 & \varepsilon' < w \sim \text{Work function} \\ \left(\dfrac{\varepsilon' - w}{\varepsilon_p - w}\right)^p & w \leqslant \varepsilon' \leqslant \varepsilon_p \sim \text{Energy of the peak production} \\ & \text{rate} \\ \left(\dfrac{\varepsilon_0 - \varepsilon'}{\varepsilon_0 - \varepsilon_p}\right)^q & \varepsilon_p < \varepsilon' \leqslant \varepsilon_0 \\ & p, q \geqslant 0 \sim \text{Adjustable constants}. \end{cases} \qquad (12)$$

with

$$B = \left[\frac{\varepsilon_p - w}{p+1} + \frac{\varepsilon_0 - \varepsilon_p}{q+1}\right]^{-1} \sim \text{Normalization factor}.$$

Adjustment of w, ε_p, q, and p allows the reasonable approximation of a variety of $\varrho(\varepsilon')$ functions.

Three levels of solar activity are considered. Average solar activity corresponds to the 'Solar Flux' curve in Figure 3. Variability of the differential photon flux ($\varepsilon_0 > 10$ eV) with solar activity is modeled by the factor $\phi(\varepsilon_0, r) = \phi(\varepsilon_0/10\ \mathrm{eV})^r$ where $r = 0$ for average activity, $r = -1$ quiet solar conditions, and for active solar conditions $r = +1$. This provides qualitatively correct intensity profiles to the observed ranges of the differential flux in the 44–60 Å and 8–12 Å bands.

Equation (13) specifies the integral energy flux ($E(>\varepsilon)$) conveyed into the solar wind by photoelectrons evoked by photons with energy greater than ε on emergence from the top of the photoelectron layer. The ε-value of a photoelectron is $(e \cdot U_{\mathrm{pel}} + w)$ lower at the escape layer than in the surface: namely,

$$E(>\varepsilon) = \cos\alpha \frac{G}{2\pi} \int_{\varepsilon > \varepsilon_b + w}^{\varepsilon'} \int_{\varepsilon'}^{\infty} (\varepsilon' - \varepsilon_b - w) \times$$

$$\times Y(\varepsilon_0)\, \varrho\left(\frac{\varepsilon'}{\varepsilon_0}\right) [\phi(\varepsilon_0)\,\mathrm{d}\varepsilon_0]\,\mathrm{d}\varepsilon' . \qquad (13)$$

Formation of a shock streamer requires that $[E(>\varepsilon_b)/F_{\mathrm{sw}}] > \bar{\varepsilon}_s = (\eta + \Delta\eta)/N$. That is, sufficient photoelectron energy must be provided to replace the normal energy density of the solar wind electrons and generate the required pressure in the solar wind necessary for shock production.

4. Specific Models of Photoelectron Production

In this section experimental and theoretical information available for modeling of the photoelectron production rates and energy flux is presented. Numerical results for the two basic models are tabulated and discussed.

A. LUNAR SURFACE (CPLEE) MODEL

Reasoner and Burke (1972) have inferred a differential energy spectrum for the 40–200 eV lunar photoelectrons of the form $f(\varepsilon')=f_0(\varepsilon'/\varepsilon_1')^{-K}$ where $\varepsilon_1' \simeq 40$ eV, $f_0 \simeq 3\times 10^5$ electrons cm^{-2} s^{-1} ster^{-1} eV^{-1} and $K \simeq 3.5$–4.0. This spectral model is based on data from the Charged-Particle Lunar Environment Experiment (CPLEE) which was emplaced on the lunar surface during the Apollo-14 mission.

The Moon was in the magnetotail when the spectrum was obtained. Thus, all the photoelectrons were returned to the surface. Previous theoretical treatments of the situation have been provided by Walbridge (1970) and Singer and Walker (1962). The observed spectrum will be reasonably similar to that expected for the photoelectron surface flux ($F(>\varepsilon)$). Their measurements indicate an outward photoelectron energy flux of 1.5 to 3×10^9 eV cm^{-2} s^{-1} conveyed by electrons with energies between 40 and 200 eV at 25 cm above the lunar surface.

The parameters in Equation (12) were taken as $w=6$ eV, $\varepsilon_p=(w+\varepsilon_0)/2$, and $p=q=1$ to approximate the expressions assumed by Reasoner and Burke in their model calculations. $Y(\varepsilon_0)$ is approximated by $Y(<6\text{ eV})=0$, $Y(6\leqslant\varepsilon_0\leqslant 9)=$ $=0.1(\varepsilon_0-6)/3$, and $Y(>9\text{ eV})=0.1$. Figures 5, 6, 7, and 8 summarize the results of these calculations for the CPLEE-model. The Figure 5 caption describes the nomenclature and parameters.

It is the contention in this paper that under most conditions the flatland photoelectrons will cool the solar wind and suppress shocks whereas under certain conditions (active Sun and low ε_{sw}, N, and B_{sw}) major highland features will produce shocks by the injection of hot photoelectrons. Figure 5 confirms the plausibility of this theory. For normal and quiet solar conditions neither the flatlands nor the highlands will inject sufficient energy into the quiet, average, or fast-disturbed solar wind to produce a shock. Under active solar conditions ($r=+1$) highland shocks can be expected for all solar wind conditions except a fast-disturbed flow with an increase magnetic field. Shocks are most easily produced under very quiet conditions, $N\simeq 4$, and $B_{sw}\simeq 1.8\ \gamma$. Highland will evoke shocks under active or normal Sun conditions and a 'whole-Moon' shock could be produced under active Sun conditions ($r=+1$, $\alpha=89.50$).

Figure 6 displays the dependence of the average energy (ε_{ph}) in electron-volts of an escaping photoelectron versus the accretion flux of solar wind electrons. The interpretation is identical to that for Figure 5. A shock will occur if $\varepsilon_{ph}>\varepsilon_s$; local streaming turbulence but no shock occurs for $\varepsilon_s>\varepsilon_{ph}>\varepsilon_{sw}$; and smoothed flow with no shock occurs for $\varepsilon_{sw}>\varepsilon_{ph}$. For the observed range of F_{sw} the photoelectron energy (escape) will vary over the wide range $\varepsilon_{ph}\simeq 0.06$–112 eV depending on lunar geography and solar activity. Thus, a wide range of ε_{sw} and ε_s values can be accommodated.

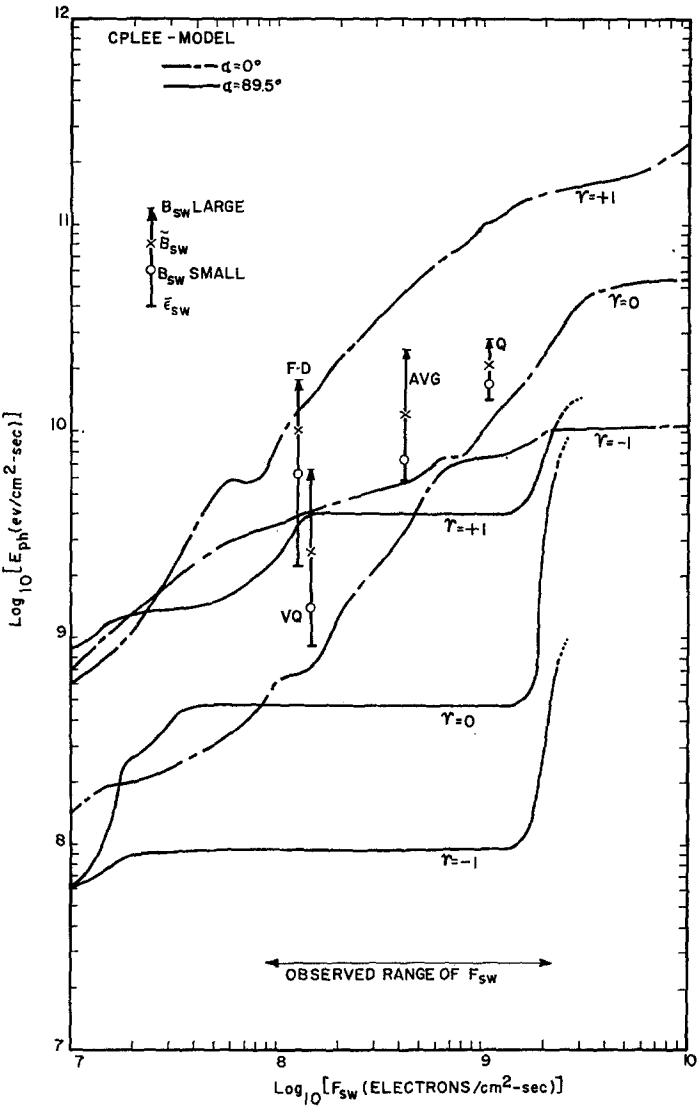

Fig. 5. This graph displays the energy transported into the solar wind [E_{ph}(eV/ cm— s)] by photoelectrons versus the accretion flux of solar wind electrons [F_{sw} (electrons cm^{-2} s^{-1})] for the CPLEE-model. The parameters are Sun angle (α) of the terrain ($\alpha = 0° \sim$ vertical cliff, $\alpha = 89.5° \sim$ flatland with the solar disk just on the local horizon) and solar activity ($r = -1 \sim$ quiet Sun, $r = 0 \sim$ normal Sun, and $r = +1 \sim$ active Sun; refer to the text following Equation (9)). The vertical lines indicate the four qualitative states of the solar wind (VQ ~ very quiet, Q ~ quiet, AVG ~ average, and F-D ~ fast-disturbed) presented in Table I. Note the coding of the vertical lines. The base (ε_{sw}) corresponds to the normal energy input by accreting solar wind electrons; 'x' denotes the outward energy flux required for shock production for the average value of B_{sw} while the top of the line and '○' indicate shock conditions for B_{sw} values differing by $\pm 1\sigma$ from average.

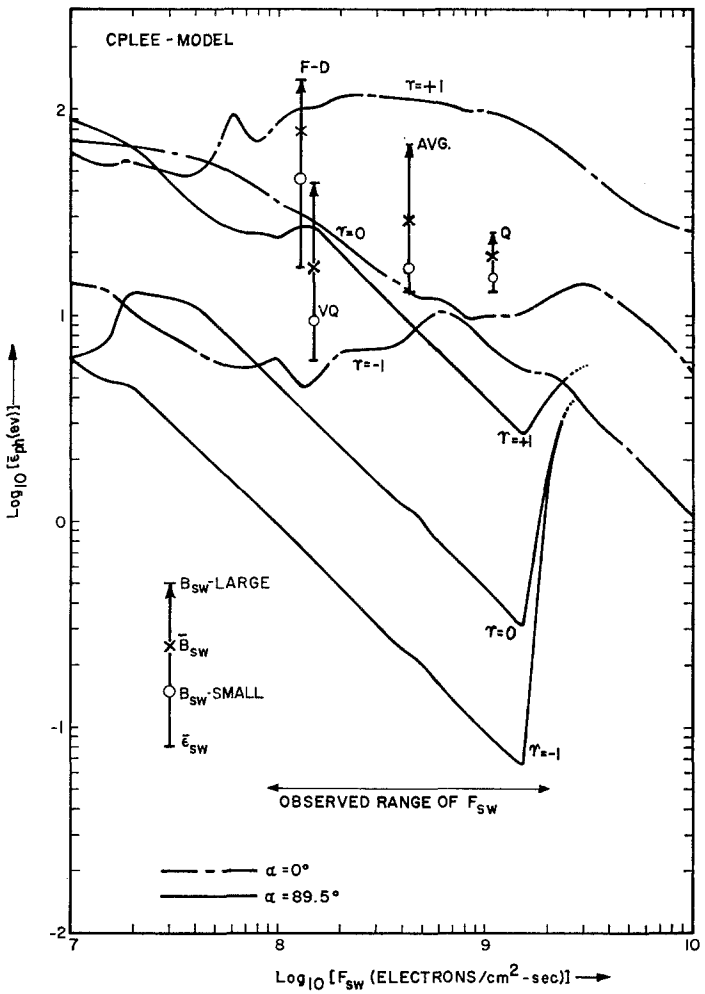

Fig. 6. This graph displays the average energy (ε_{ph}) of photoelectrons escaping into the solar wind. All other conditions and notations are the same as Figure 5. The dashed portion of the $\alpha = 89.5°$ curves indicate maximum photoelectron current for the specified conditions.

Figure 7 is useful for understanding the major variations of the curves in Figures 5 and 6. As before, F_{sw} is the abscissa. The sum of the surface work function (w) and the electrical potential difference (U_{pel}) between the lunar surface and the photoelectron/solar wind interface is the ordinate. Photoelectrons with total energy (ε) at the surface such that $\varepsilon < (eU_{pel} + w)$ will not escape into the solar wind but will be returned to the surface. Conversely, escaping photoelectrons must have $\varepsilon > eU_{pel} + w$ which means they are produced by protons with $\lambda(\text{Å}) \leqslant 12000/(eU_{pel} + w)$. Notice that the $\alpha = 89.5°$ curves converge to $U_{pel} = 9.9$ V over most of the observed range of F_{sw}. Convergence occurs because solar Lα ($\lambda = 1216$ Å or $\varepsilon_0 = 10.2$ eV) dominates the integral solar flux for $\varepsilon_0 > 10$ eV and thus the production of photoelectrons. The

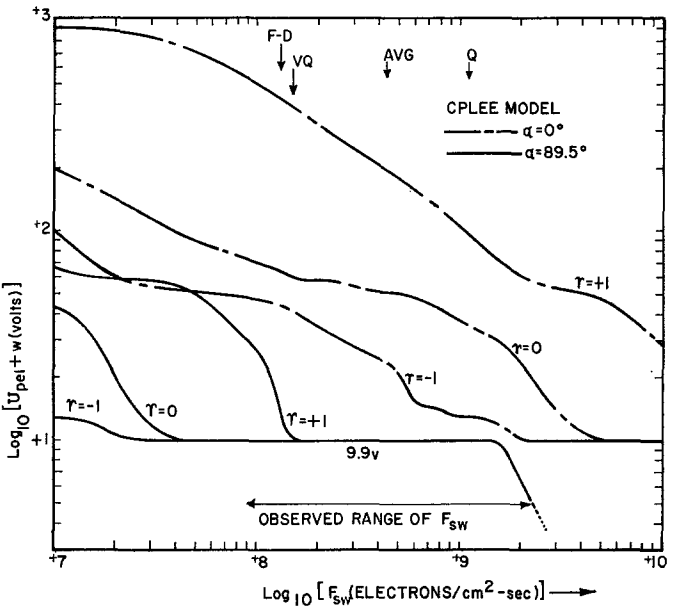

Fig. 7. This graph displays the sum of the work function w/(eV) and the potential difference between the lunar surface and the photoelectron/solarwind interface approximately one Debye length above the surface (Equation (13)). The conditions and nomenclature of Figure 5 apply.

photoelectrons induced by Lyman-α(Lα) constitute a large reservoir which can trade-out many photoelectrons before suffering a significant change in the average energy of the 'reservoir' electrons. This Lα reservoir is the reason $\alpha = 89.5°$ curves of ε_{ph} decrease monotonically in Figure 6 until the reservoir is depleted and similarly for $F_{sw} > 2 \times 10^9$ cm^{-2} s^{-1} for the $\alpha = 0°$, curves where $r = 1$, and $r = 0$.

The very large reservoir of Lα photoelectrons forces ε_{ph} down until the reservoir is exhausted (bottom of the curve for $\alpha = 89.5°$, $r = -1$ in Figure 6) and then allows a subsequent increase of ε_{ph} as F_{sw} continues to increase.

Suppression of ε_{ph} by large values of U_{pel} is the reason the ($\alpha = 0°$, $r = +1$) curve in Figure 6 peaks inside the observed range of F_{sw} rather than for smaller F_{sw} values. Notice for the corresponding curve in Figure 7 that $U_{pel}(F_{sw} = 2 \times 10^7$ cm^{-2} s$^{-1}) \simeq$ $\simeq 900$ V whereas $U_{pel}(F_{sw} = 3 \times 10^8$ cm^{-2} s$^{-1}) \simeq 230$ V.

The $\alpha = 89.5°$ curves in Figures 5, 6, and 7 terminate in dashed lines which indicates the maximum photoelectron production or the saturation photocurrent. For areas where $F_{sw} > {}_{max}F$ (photoelectrons) the cool photoelectrons ($\simeq$4–6 eV, see Figure 6) will replace the most energetic solar wind electrons. The remaining solar wind electrons will be repelled by a slight negative surface charge.

The foregoing arguments have applied for $\alpha = 0°$ and 89.5°. Obviously, vertical slopes with 1–2 km high faces will not be common lunar features. Figure 8 (a, b, and c) presents the variations of ε_{ph} versus α for the F_{sw} values corresponding to quiet, average, and fast-disturbed flows. The pertinent feature of these curves is the con-

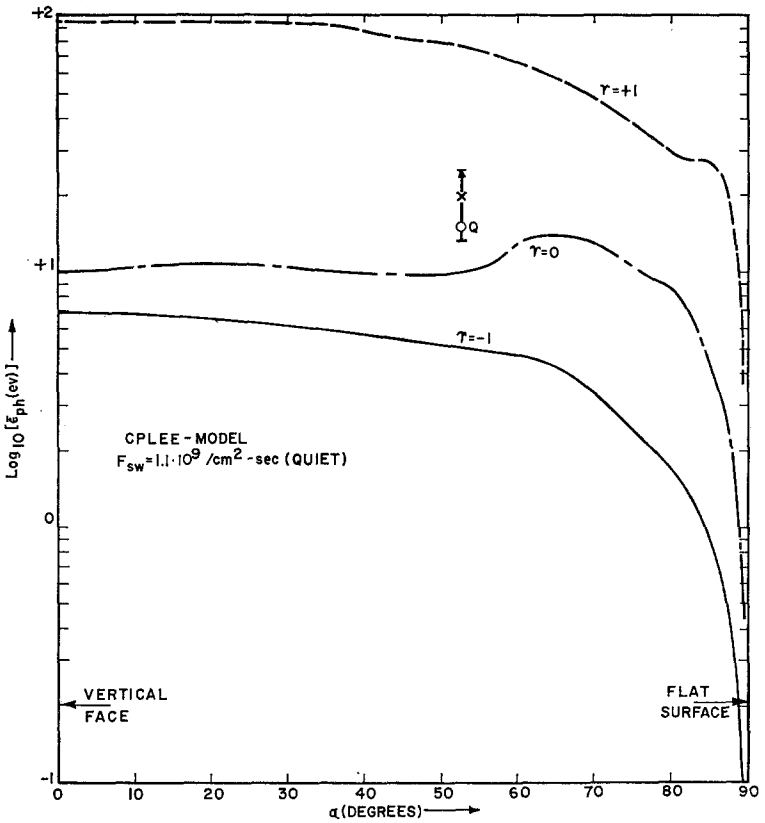
+2
+1
0
-1
τ=+1
τ=0
τ=-1
Q
CPLEE-MODEL
F_{sw}=1.1·10^9 /cm^2-sec (QUIET)
VERTICAL FACE
FLAT SURFACE
Log$_{10}$[E_{ph}(ev)]
0 10 20 30 40 50 60 70 80 90
α(DEGREES)

(a)

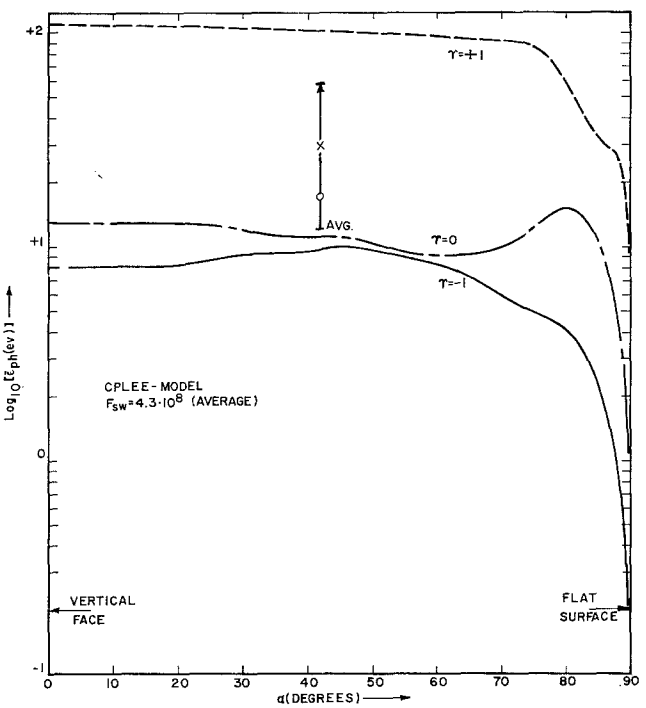
+2
+1
0
-1
τ=+1
τ=0
τ=-1
AVG.
CPLEE-MODEL
F_{sw}=4.3·10^8 (AVERAGE)
VERTICAL FACE
FLAT SURFACE
Log$_{10}$[E_{ph}(ev)]
0 10 20 30 40 50 60 70 80 90
α(DEGREES)

(b)

Fig. 8a, b.

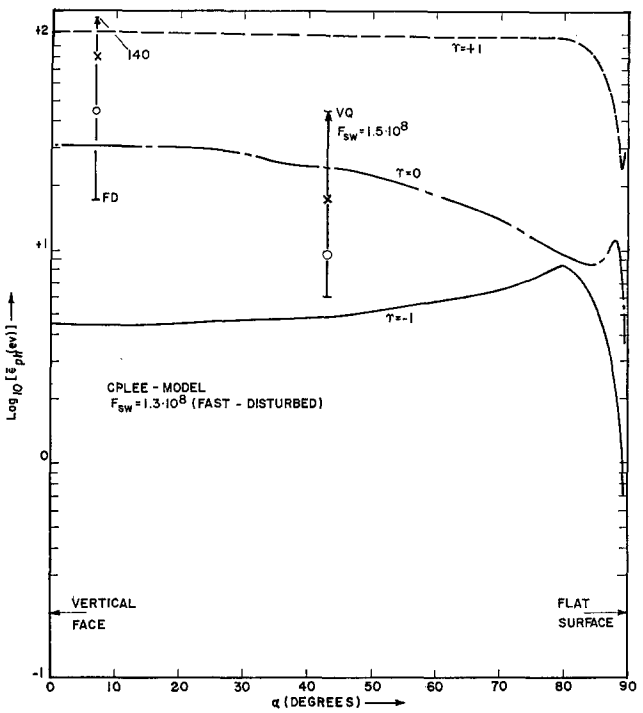

Fig. 8. Average photoelectron energy (ε_{ph}(eV)) is plotted versus α (degrees) for three values of the accretion flux of solar wind electrons. The parameter r indicates the level of solar activity [quiet (-1), normal (0), active ($+1$)].

stancy of ε_{ph} over wide ranges of α. In Figure 8a one sees that ε_{ph} actually increases from 10 eV at $\alpha=0°$ for the $r=0$ (normal Sun) case to 14 eV at $\theta=65°$. These curves indicate that local surface slopes (slope angles $\chi=90°-\theta$) in the range of 10°–20° will be capable of evoking shocks under certain solar wind conditions and that $\chi=40°$ slopes are as effective as $\chi=90°$ slopes in evoking shocks. Notice also the very sharp drop in ε_{ph} for $\theta>80°$ or $\chi<10°$ for most of the curves. Under most F_{sw}-values and solar conditions those surfaces with slopes less than 10° should generate only low energy photoelectrons and thus cool the solar wind.

This result seems inconsistent on first glance with the simple exchange model presented in Section 2. After all, the number of high energy photoelectrons should decrease as cosα and produce a smooth decrease in ε_{ph}. This argument is correct for the photoelectron flux leaving the lunar surface. However, the photoelectrons escaping into the solar wind lose energy passing through the potential drop across the photoelectron layer. The variation of $[eU_{pel}+w]$ with α is shown in Figure 9 for $F_{sw}=4.3\times10^8$ cm^{-2} s^{-1} (Figure 8b). Notice that $[eU_{pel}+w]$ decreases monotonically as α increases. The effect of $[eU_{pel}+w]$ is to suppress ε_{ph} strongly at $\alpha=0°$ but to be less suppressive as α approaches 90°. Overall, ε_{ph} is reduced and made reasonably insensitive to α for $\alpha<80°$ which corresponds to slope angles greater than 10°.

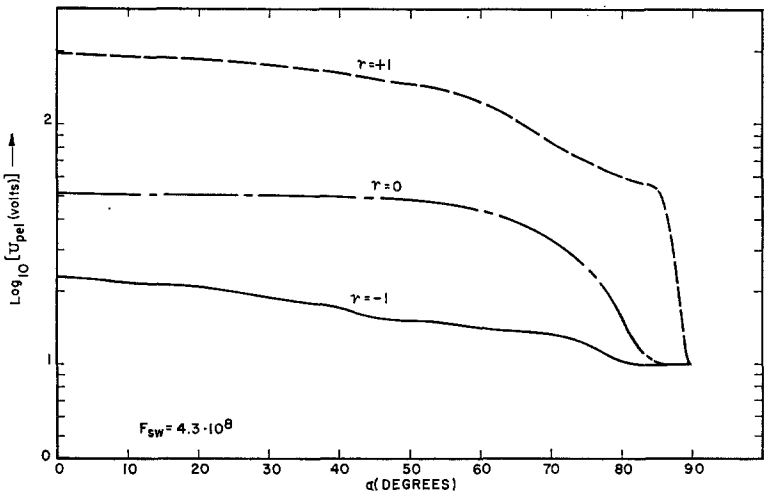

Fig. 9. The variation of the potential energy drop across the photoelectron layer $[eU_{\mathrm{pel}} + w]$ (V) versus α is shown for the average value of the electron accretion flux of the solar wind. The parameter r indicates the level of solar activity [quiet (−1), normal (0), and active (+1)]. The ordinate is incorrectly labeled as $\log_{10}[eU_{\mathrm{pel}}(\mathrm{eV})]$.

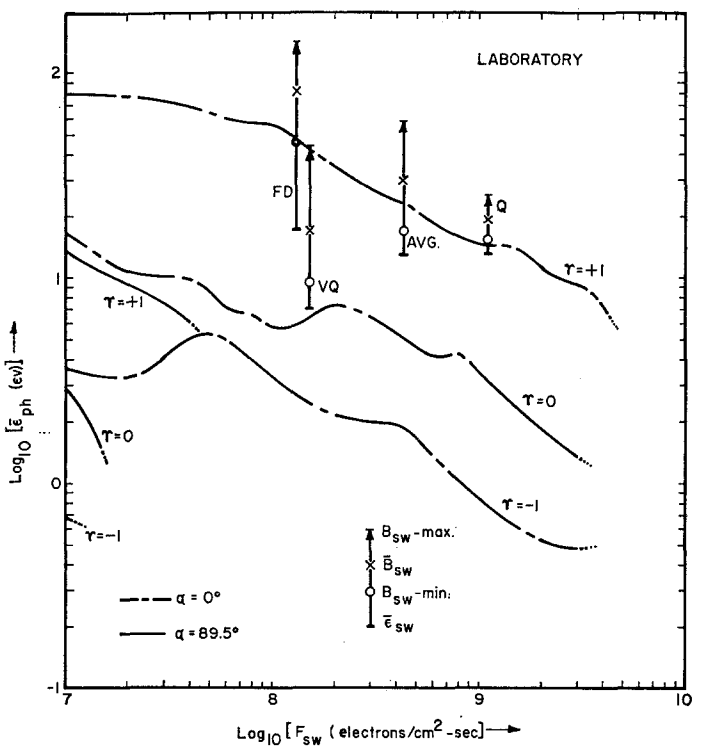

Fig. 10. The average energy of escaping photoelectrons ($\varepsilon_{\mathrm{ph}}$(eV)) is plotted versus the solar wind accretion flux (F_{sw} (electrons cm^{-2}—s^{-1})) for the parameters of photoelectron yield and energy distribution established by Feuerbacher *et al.* (1972). Refer to the Figure 5 caption for nomenclature.

B. LABORATORY MEASUREMENTS

Feuerbacher *et al.* (1972) obtained experimental values for Y ($4\text{ eV} < \varepsilon_0 \lesssim 20\text{ eV}$) and ϱ ($0\text{ eV} < \varepsilon' < 13\text{ eV}$) for a returned sample of lunar fines (#14259,116). Their data will be approximated by

$$Y = \begin{cases} 0 & \varepsilon_0 < 5\text{ eV} \\ (0.07)\,[7/(\varepsilon' - 5)]^{-5.147} & 5 \leqslant \varepsilon_0' \leqslant 12\text{ eV} \\ 1.5 \times 10^{-2} & \varepsilon_0' > 12\text{ eV}. \end{cases}$$

Equation (12) for $\varrho(\varepsilon'/\varepsilon_0)$ is approximated by setting $w = 5$ eV, $p = 2$, $q = 3$ and

$$\varepsilon_p = \begin{cases} (5/7)\,(\varepsilon_0 - 12) + 10 & 5 \leqslant \varepsilon_0 \leqslant 12\text{ eV} \\ 10\text{ eV} & \varepsilon_0 > 12\text{ eV}. \end{cases}$$

The photoelectron spectrum resulting from the 'laboratory measurements' will produce fewer total electrons (saturation photocurrent $\simeq 3 \times 10^9$ electrons $\text{cm}^{-2}\,\text{s}^{-1}$ for normal Sun) and proportionally more low energy electrons than the 'CPLEE' model (saturation current $\simeq 3 \times 10^{11}$ electrons $\text{cm}^{-2}\,\text{s}^{-1}$).

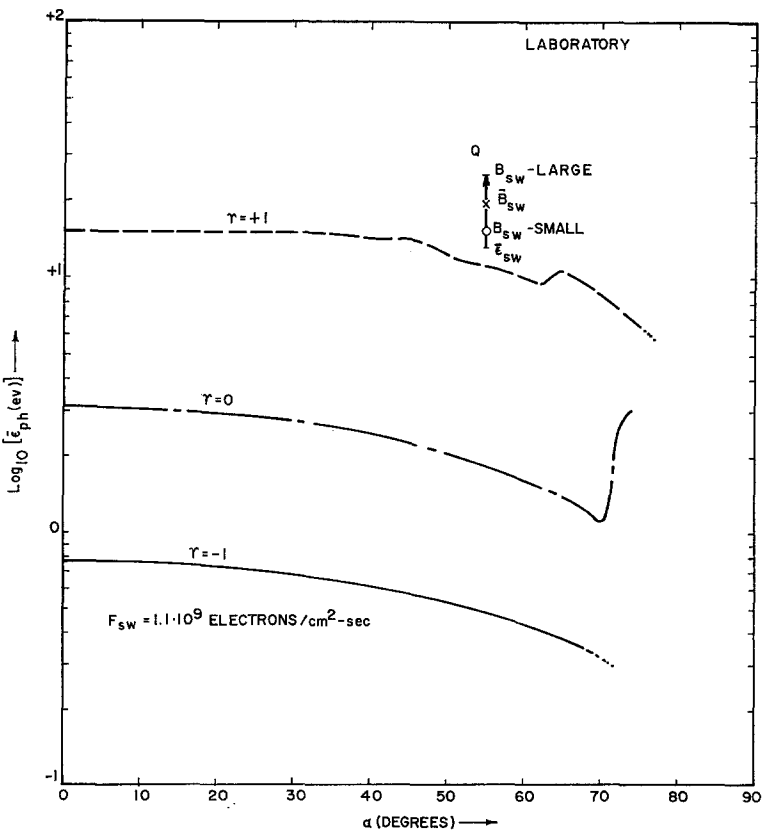

Fig. 11a.

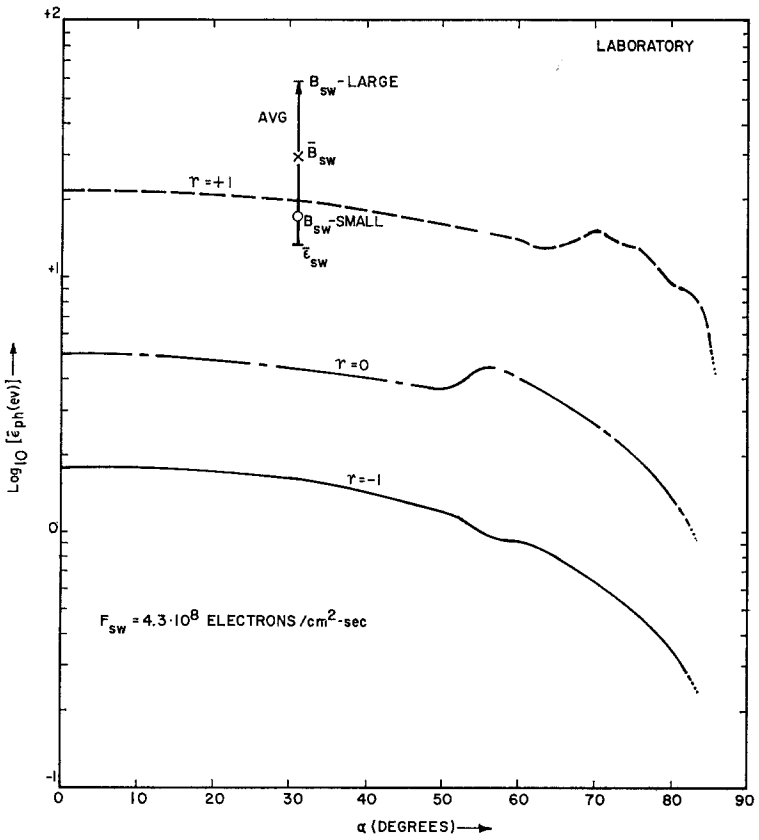

Fig. 11b.

Figure 10 reveals the dependence of ε_{ph} on F_{sw}. For vertical surface features ($\alpha=0°$) an extremely active Sun ($r \geqslant 1$) is required to evoke shocks for all but the very quiet (VQ) solar wind conditions. Intermediate solar activity ($0<r<1$) should evoke shocks for the very quiet solar wind flow. Flatlands electrons ($\alpha \simeq 89.5°$) will be unable to replace solar wind electrons because of the low saturation currents.

Figure 11 (a, b, c) shows the dependence of ε_{ph} on α for the three typical solar wind conditions. In a general sense these curves are similar to those in Figure 8. ε_{ph} does not monotonically decrease with increasing α until $\alpha(\gtrsim 70°)$ is large. The insensitivity of ε_{ph} on α results from the monotonic decrease of U_{pel} with α. However U_{pel} will be a factor of 5 or more smaller for given F_{sw}, r, and α values in the 'Laboratory' case than as shown in Figure 7.

Very little data exist on Y and ϱ appropriate to materials which are insulators or those that occupy the transition region between insulators (basically ionic electrical conductors) and semiconductors (electronic conductors). Electrical conductivity measurements ($\simeq 10^{-17}$ mhos cm^{-1} at 0 °C and 0 Hz) place the lunar rocks in the insulator class (Strangway *et al.*, 1972). Theoretically, insulators should possess high yields.

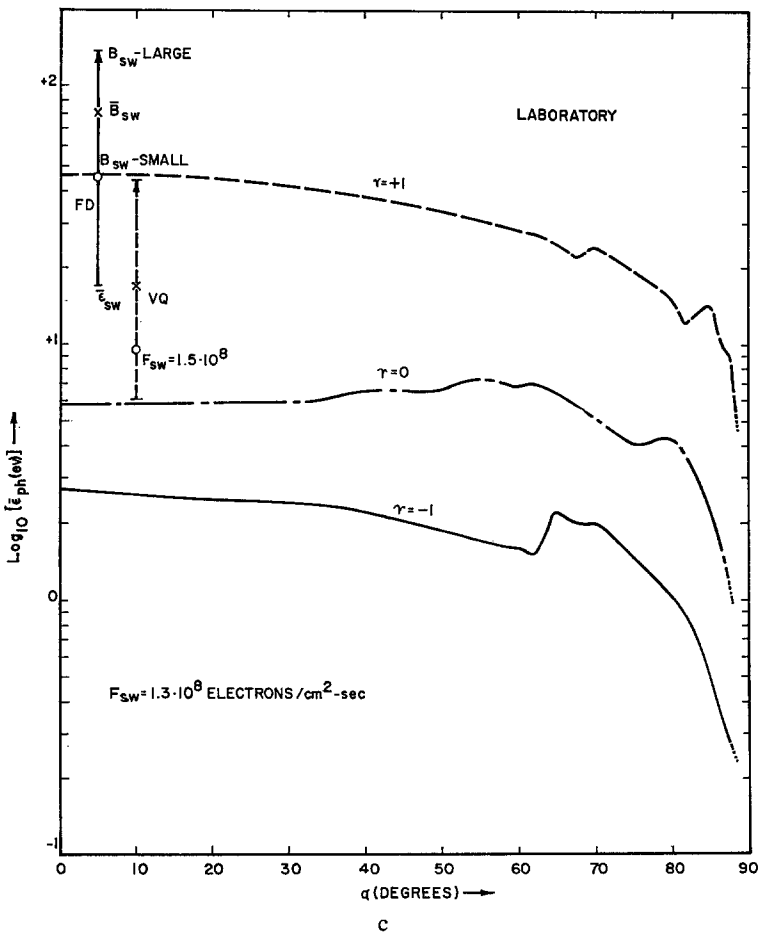

Fig. 11. Average photoelectron energy (ε_{ph}(eV)) versus α (degrees) based on the 'Laboratory parameters. Refer to the Figure 8 caption for details.

Many of the photoelectrons should possess energies near either the photon energy or the band gap energy (E_g) of the material due to the absence of conduction band electrons which would effectively scatter the photoelectrons and degrade their energy (Spicer, 1968). Experimentally, $Y \gtrsim 1$ are observed for photon energies $h\nu \gtrsim E_g$. Y displays a relative minimum at E_g and increases thereafter as photoelectrons ionize and eject other bound electrons while escaping from the material (Sommer, 1968; Metzger, 1965). Taylor and Hartman (1959) and Newburgh (1963) have observed these effects in NaCl, KCl and LiF and observe the production of many very low energy (<2 eV) photoelectrons for $h\nu < 21$ eV which is $< 2E_g$. For higher photon energies the fraction of photoelectrons with $\varepsilon \lesssim \frac{1}{2}\nu$ appears to increase. This may happen on the Moon for $h\nu > 20$ eV.

The possibility must be seriously considered that contamination of lunar samples by even transient exposure to atmosphere, especially water vapor, irreversibly increases

the abundance of conduction band electrons. Alverez (1972), on the basis of vacuum experiments with hematitic sandstone, indicates that changes in surface conductivity due to fractional monolayers of water is not described by aqueous electrolytic conduction on the surface. Variation in the surface semiconduction properties is hypothesized. Strangway *et al.* (1972) has observed a 10^4 increase in the zero-frequency conductivity of lunar fines following short exposure of the sample to a humid atmosphere. These considerations support the view that the CPLEE model is more suited to in situ photoelectron production than the laboratory model.

5. Shock Model and Lunar Terrain

How high must a mountain or highland extend and what must the average slope be in order to induce shock streamers? The Moon accretes solar wind electrons with guiding centers which pass within approximately one electron cyclotron radius (r_e) of the terminator surface when V and B_{sw} are parallel. The solar wind flux per unit of latitude length (dF/dl) through this adsorption annulus is given approximately by $dF/dl \simeq (Nv_t/2\pi^{1/2})r_e$ (refer to Equation (7)). Mountain slopes or sets of slopes of summed height (h) must provide the replacement flux. That is $dF/dl = Fh$, where F is the escaping photoelectron flux per unit of surface area. In the solar wind section we noted that $F \simeq Nv_t/2\pi^{1/2}$. Therefore, for flux balance we have $r_e \simeq h$. From Table I we have $\simeq 5.2\gamma$ and $2.2\gamma < B < 9.9\gamma$ with very little systematic dependence of B on V or N. Electron thermal velocity ($v_t \simeq 2.2 \times 10^3$ km s^{-1}, $1.3 \times 10^3 < v_t$ (km s^{-1}) $< 2.2 \times \times 10^{+3}$) is also insensitive to solar wind conditions. Thus, $\mathbf{r}_e \simeq 2.2$ km and 0.74 km $< r_e <$ 5.7 km is the approximate range for r_e and h.

Figure 12 (Wollenhaupt and Sjogren, 1972; and Kaula *et al.*, 1972) presents the deviation of the lunar surface under the ground track of the Apollo-15 CSM from a spherical-Moon model (ΔR km). Measurements were obtained by a laser altimeter approximately every 33 km along the ground track. Elevation differences of 2 to 6 km are present in distances less than 30–100 km. Thus, the Moon does possess sufficient elevation differences to provide a replacement flux of photoelectrons for the solar wind electrons accreting from the transition region. Furthermore, the greatest elevation differences (60° E–105° E, 140° E–150° N) are associated with regions which produce shock streamers.

The middle and bottom sections of Figure 12 illustrate the available data on variation of shock-streamer production and the slope of the lunar surface. Regions of greatest slope ($\chi > 6°$ in areas (1), (2), (3), and (4)) are associated with shock production. It must be remembered that these χ-values are obtained by discrete elevation measurements which are separated by approximately 33 km. Extensive analysis of terrain photography will be required to establish the actual slopes of major features in these areas. 'χ' of many of the illuminated slopes should be larger than indicated by Figure 12 due to terracing or similar relief patterns.

Conversely, most regions with $\chi < 6°$ display small or zero occurrence rates of shock production. Agreement is not complete. Regions (5) and (8) produce shocks whereas

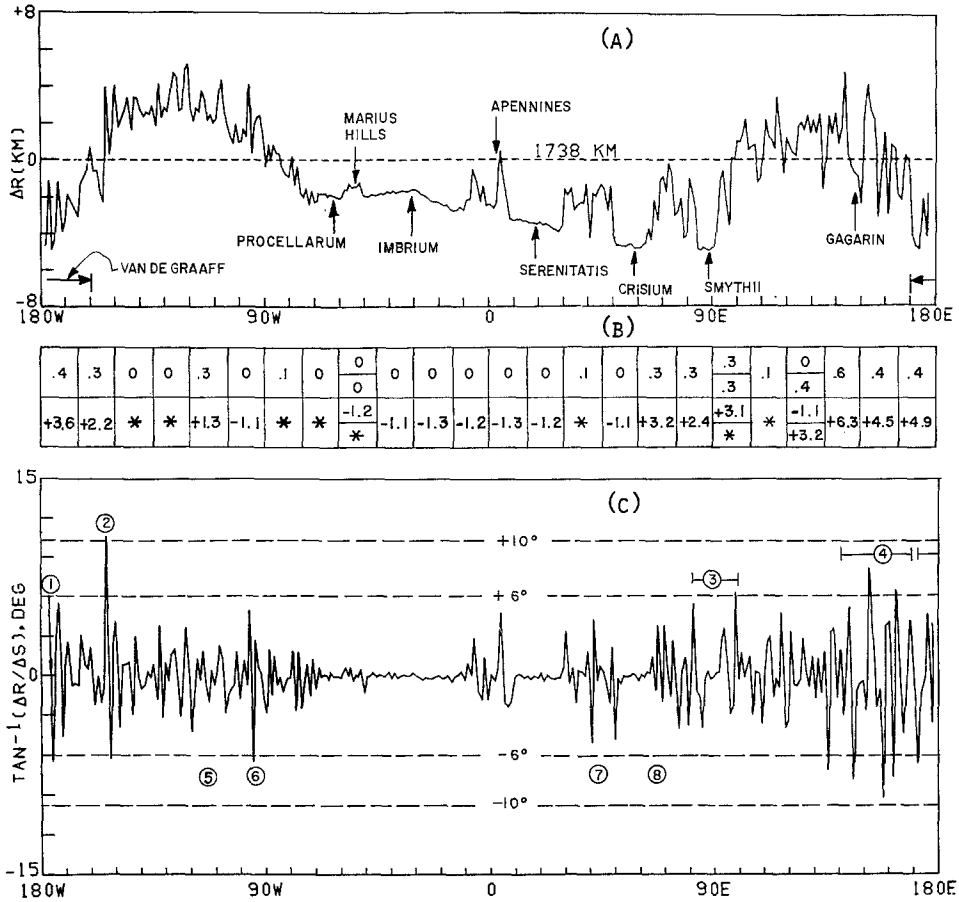

Fig. 12. Part (a) displays the deviation of the lunar surface from a sphere of 1738 km radius as measured along the Apollo-15 CSM ground track by the laser altimeter. Part (c) is the surface slope in degrees derived from the elevation measurements which were separated by 33 km. The top line of part (b) is the fraction of times shock streamers are observed by Explorer 35 in the 15 by 15 degree box intersected by the CSM ground track (refer to Figure 3). The bottom line is the statistical significance assigned to the fractional value.

regions (6) and (7) have large slopes and do not evoke shocks. Detailed stereophotography of these regions must be examined in order to determine the actual slopes. It should be re-emphasized that while an intense and localized remanent magnetic field (refer to Figure 3) is associated with the strong production region near Van De Graaff (1) there are not similar magnetic fields associated with the Gagarin and Levi Civita regions (4) which are detectable at an altitude of 100 km. However, the large slope values and corresponding elevation changes are similar in the two regions.

There should be a minimum face length along (i.e., in latitude) the terminator for shock streamer production. Certainly, $r_e \simeq 0.7$–6 km is the minimum range and easily achievable. Shock production areas have been localized to 15° or less on a side. Thus,

the characteristic length of the source region need not be greater than 450 km. It is reasonable to expect an extensive region to be more effective than a localized region in the production of shocks.

6. Discussion

Several experimental and theoretical facets of the limb shock problem must receive qualitative elaboration. Sonett and Mihalov (1972) maintain there is a statistically significant deficiency of high latitude ($>30°$ N or S) shock streamers (refer to Figure2). The deficiency is, on first consideration, inconsistent with the electron-exchange model. The poleward surface is rugged and must contain vertical features comparable to those in the 30° N–30° S lat. band. It is suggested here that the exchange model is correct but that electron heat conduction along B_{sw} controls the appearance of downstream shocks. Low latitude shock streamers will be intersected by magnetic field lines which pass through the downstream void region (refer to Figure 1). Electron heat flow is stopped at the void/wake interface due to the absence of conduction electrons in the void (Serbu, 1969). However, magnetic field lines which pass through only the wake region will conduct electron heat from (or to, as the case may be) the wake/solar wind interface. Heat conduction, nominally $H_0 = 4 \times 10^9$ eV cm^{-2} s^{-1} in the solar wind (Ogilvie *et al.*, 1971), will be reduced because $N(\text{wake})/N(\text{solar wind}) \leqslant 0.1$. Assuming $H = 0.1 H_0$ the absolute lower limit which a shock region can move downstream (ds) before having its excess electron thermal energy conducted away is

$$d_s \simeq V r_e (\varepsilon_s - \varepsilon_{sw})/H \simeq 20 \text{ km or } \tau_s \simeq 5 \times 10^{-2} \text{ s (streaming time).}$$

This field line must also conduct the background heat flow of the solar wind (i.e., H_0); thus, 20 km is certainly a lower limit. The void region has a downstream radius $R_v \simeq 0.5$–$0.8\ R_m$; thus, shock streamers will be confined equatorward of lunar latitudes arcsin $(R_v/R_m) \simeq 30°$–$50°$ (Whang, 1969; Spreiter *et al.*, 1970; and Wolf, 1968) which is roughly consistent with the observations.

Figure 3 clearly indicates that electron-exchange is considered to be confined to those electrons passing within r_e ($\simeq 0.8$–5 km) of the terminator for B_{sw} parallel to V. Colburn *et al.* (1971) state there is a slight tendency (probability $\simeq 0.8$) for shock streamers to occur when B_{sw} and V are parallel. However, B_{sw} on the average makes a 45° angle to V. Thus, under most conditions thermal electrons will have a velocity along B_{sw} the order of 10^8 cm s^{-1} which should allow electrons access to the terminator and preterminator regions from solar wind streamlines many r_e away from the limb. Conversely, photoelectrons could escape to streamlines several r_e from the limb and dissipate their energy over a volume sufficiently large to force $\Delta\eta$ (the excess energy density) to zero. This will not happen if the 'mean free paths (λ_e)' of the solar wind 'plasma electrons' (<340 eV ~ Ogilvie *et al.*, 1971) and photoelectrons are the order of r_e or less. Serbu (1969) noted solar wind plasma electrons are present along the lunar wake region ($\lesssim$ few hundred eV) 1.5–5 R_m downstream of the Moon. Conversely, Anderson *et al.* (1972) find pronounced lunar shadowing effects for energetic

(>500 eV) electrons when $\cos^{-1}(\mathbf{B}_{sw}\cdot\mathbf{V})\simeq 45°$. These experimental observations argue that plasma electrons are tied closely to specific volume elements of the streaming solar wind protons, whereas, energetic electrons (>500 eV) stream freely along $\mathbf{B}_{sw}$. A value of $\lambda_e \simeq r_e$ is necessary in the vicinity of the Moon for the exchange theory to be applicable. Theoretical estimates of λ_e are not available. A lower limit would be $\lambda_e \simeq \lambda_D \simeq 10$ m.

Barnes *et al.* (1971) suggested that lunar surface magnetic fields of scale lengths $L > L_0 = Ac/\omega_p \simeq 10$ km ($A \simeq 5$, $c = 3\times 10^{10}$ cm s^{-1}, $\omega_p^2 = 4\pi ne^2/m \sim$ electron plasma frequency) produce shock streamers. L_0 is the thickness of an ion-wave shock according to the theory of Tidman (1967). Theoretically the occurrence of an ion-wave shock, which is a type of two-stream instability, does not depend on the presence of a magnetic field. The critical factors are the relative peak energies of the proton and electron thermal populations before (ε_1^+ and ε_1^-) the shock and the pre and post shock bulk velocities ($V_1 > V_2$). Qualitatively, for a shock to occur $\varepsilon_1^- > \varepsilon_1^+$ whereas for $\varepsilon_1^- < \varepsilon_1^+$ no shock will occur. In the solar wind $T_e \simeq T_i$ for disturbed conditions and $T_e \simeq$ (2 to 6) T_i for quiet conditions (Hundhausen, 1970). Figures 8 and 11 show that photoelectron ejected from highlands and flatlands into the preshock region are of the appropriate energies to satisfy both conditions. Additionally, the ion-wave process allows for the downstream development of strong shocks while permitting the decay of weak shocks (Sonett and Mihalov, 1972; Whang and Ness, 1972). Further application of the ion-wave theory to the phonemenon of lunar shocks is clearly justified.

Previous theoretical works on Moon/solar wind interaction have assumed the Moon to be a perfect adsorber of solar wind particles and have then proceeded to apply various single-particle or continuum magnetohydrodynamo theories to the downstream flow. These models are all deficient because they have not considered the possibility of active boundary conditions at the lunar terminator. There is a flow of electron thermal energy between the solar wind and the Moon. If net thermal energy flows to the moon then the solar wind flow about the Moon is smoothed and shocks do not form. If sufficient thermal energy is conveyed into the solar wind by lunar photoelectrons then a local shock streamer is formed. The boundary conditions for Moon/solar wind interactions are active. Critical parameters are the slope of the lunar surface in the terminator zone, photoelectric properties of the lunar surface, solar wind electron energy, electron density and magnetic field strength, and the general level of solar activity. Available experimental reports on lunar shocks have not presented the exact combination of variables necessary to support or reject this theory.

Assuming the general concepts of this paper are correct, one must conclude that investigations of Moon/solar wind interactions have just begun to mine rich leads of information on plasma theory (two-stream instability), heat flow properties of the solar wind, interaction scale-lengths in the solar wind and, the roles of lunar topography and lunar photoelectric properties. Photoelectron exchange theory may also be important in theories of solar wind interaction with Mercury, the asteroids, comets, and other planetary satellites.

Acknowledgements

It is a sincere pleasure to contribute to this volume in honor of Professor Urey. I am especially grateful to Mr J. Barrios for preparing the computer program utilized in this analysis. This work was done at the Lunar Science Institute, which is operated by the Universities Space Research Association under Contract No. NSR-09-051-001 with the National Aeronautics and Space Administration. This paper constitutes Lunar Science Institute Contribution No. 129.

References

Alverez, Roman: 1972, 'Electrical Conduction Phenomena in Rocks', Ph. D. dissertation, Engineering Science, Univ. of California at Berkeley.

Anderson, K. A., Chase, L. M., Lin, R. P., McCoy, J. E., and McGuire, R. E.: 1972, *J. Geophys. Res.* **77**, 4611–4626.

Barnes, A., Cassen, P., Mihalov, J. D., and Eviatar, A.: 1971, *Science* **172**, 716–718.

Clay, D. R., Goldstein, B. E., Neugebauer, M., and Snyder, C. W.: 1972, *Apollo 15 Preliminary Science Report*, NASA-SP-289, 10-1 10-7.

Colburn, D. S., Mihalov, J. D., and Sonett, C. P.: 1971, *J. Geophys. Res.* **76**, 2940–2957.

Colburn, D. S., Currie, R. G., Mihalov, J. D., and Sonett, C. P.: 1967, *Science* **158**, 1040.

Coleman, P. J., Lichtenstein, B. R., Russell, C. T., Sharp, L. R., and Schubert, G.: 1972, *Geochim. Cosmochim. Acta., Suppl.* **3**, 2271–2285.

Criswell, D. R.: 1973, *Proceedings of the Symposium on Photon and Particle Interactions with Surfaces in Space*, to be published.

Dryer, Murry: 1968, *J. Geophys. Res.* **73**, 3583–3584.

Feuerbacher, B., Anderegg, M., Fitton, B., Laude, L. D., Willis, R. F., and Grard, R. J. L.: 1972, *Geochim. Cosmochim. Acta., Suppl.* **3**, 2639–2653.

Freeman, J. W.: 1972, *J. Geophys. Res.* **77**, 239–243.

Gold, T.: 1966, in *The Solar Wind* (ed. by R. J. Mackin, Jr., and M. Neugebauer.), Jet Propulsion Laboratory, California Institute of Technology, Pasadena, p. 381.

Grobman, W. D. and Black, J. L.: 1969, *J. Geophys. Res.* **74**, 3943–3951.

Hinteregger, H. E.: 1970, *Ann. Geophys.* **26**, 547–554.

Hollweg, J. V.: 1968, *J. Geophys. Res.* **73**, 7269–7276.

Hollweg, J. V.: 1970, *J. Geophys. Res.* **75**, 1209–1216.

Hundhausen, A. J.: 1970, *Rev. Geophys. Space Phys.* **8**, 729–811.

Hundhausen, A. J., Bame, S. J., Ashbridge, J. R., and Sydoriak, S. J.: 1970, *J. Geophys. Res.* **75**, 4643–4657.

Johnson, F. S.: 1961, *Solar Radiation*, Stanford Univ. Press, pp. 77–84.

Johnson, F. S. and Midgley, J. E.: 1968, *J. Geophys. Res.* **73**, 1523–1532.

Kaula, W. M. Schubert, G., Lingenfelter, R. E., Sjogren, W. L., and Wollenhaupt, W. R.: 1972, *Geochim. Cosmochin. Acta., Suppl. 3*, **3**, 2189–2204.

Kreplin, Robert W.: 1970, *Ann. Geophys.* **26**, 567–574.

Lyon, E. F., Bridge, H. S., and Binsack, J. H.: 1967, *J. Geophys. Res.* **72**, 6113–6117.

Metzger, P. H.: 1965, *J. Phys. Chem. Solids* **26**, 1879–1887.

Mihalov, J. D., Sonett, C. P., Binsack. J. H., and Moutsoulas, M. D.: 1971, *Science* **171**, 892–895.

Ness, N. F., Behannon, K. W., Scearce, C. S., and Cantarano, S. C.: 1967, *J. Geophys. Res.* **72**, 5769.

Ness, N. F., Behannon, K. W., Taylor, H. E., and Whang, Y. C.: 1968, *J. Geophys. Res.* **73**, 3421–3440.

Ness, N. F., Hundhausen, A. J., and Bame, S. J.: 1971, *J. Geophys. Res.* **76**, 6643–6660.

Neugebauer, M., Clay, D. R., Goldstein, B. E., and Snyder, C. W.: 1971, *EOS* **52**, 910.

Newburgh, R. G.: 1963, *Phys. Rev.* **132**, 1570–1575.

O'Brien, B. J. and Reasoner, D. L.: 1971, *Apollo 14 Preliminary Science Report*, NASA-SP-272, 193.

Ogilvie, K. M., Scudder, J. D., and Sugiura, M.: 1971, *J. Geophys. Res.* **76**, 8165–8173.

Reasoner, David L. and Burke, William J.: 1972, *Geochim. Cosmochim. Acta., Suppl. 3*, **3**, 2639–2653.
Schwartz, K., Sonett, C. P., and Colburn, D. S.: 1969, *The Moon* **1**, 7–30.
Serbu, G. P.: 1969, *J. Geophys. Res.* **74**, 372–376.
Serbu, G. P.: 1972, *J. Geophys. Res.* **77**, 1703–1712.
Singer, S. F. and Walker, E. H.: 1962, *Icarus* **1**, 7–12.
Siscoe, G. L., Lyon, E. F., Binsack, J. H., and Bridge, H. S.: 1969, *J. Geophys. Rev.* **74**, **59**.
Snyder, C. W., Clay, D. R., and Neugebauer, M.: 1970, *Apollo 12 Preliminary Science Report*, NASA-SP-235, 75–81.
Sommer, A. H.: 1968, *Photoemissive Materials*, John Wiley and Sons, Inc., New York.
Sonett, C. P. and Colburn, D. S.: 1967, *Nature* **216**, 340.
Sonett, C. P. and Colburn, D. S.: 1968, *Phys. Earth Planet. Interiors* **1**, 326.
Sonett, C. P. and Mihalov, J. D.: 1972, *J. Geophys. Rev.* **77**, 588–603.
Sonett, C. P., Smith, B. F., Colburn, D. S., Schubert, G., and Schwartz, K.: 1972, *Geochim. Cosmochim. Acta., Suppl. 3* **3**.
Spicer, W. E.: 1968, in *A Survey of Phenomena in Ionized Gases*, International Atomic Energy Agency, Vienna.
Spreiter, J. R., Marsh, M. C., and Summers, A. L.: 1970, *Cosmic Electrodyn.* **1**, 5–50.
Strangway, D. W., Olhoeft, G. R., Chapman, W. B., and Carnes, J.: 1972, *The Moon*, submitted for publication.
Taylor, J. W. and Hartman, P. L.: 1959, *Phys. Rev.* **113**, 1421–1435.
Tidman, D. A.: 1967, *Phys. Fluids* **10**, 547–564.
Walbridge, Edward: 1970, *The Photoelectron Layer 1. The Steady State*, High Altitude Observatory, National Center for Atmospheric Research, Boulder, Colorado.
Wende, Charles D.: 1972, *Solar Phys.* **22**, 492–502.
Whang, Y. C.: 1969, *Phys. Rev.* **186**, 143–150.
Whang, Y. C. and Ness, N. F.: 1970, *J. Geophys. Res.* **75**, 6002–6010.
Whang, Y. C. and Ness, N. F.: 1972, *J. Geophys. Res.* **77**, 1109–1115.
Wolfe, R. A.: 1968, *J. Geophys. Res.* **73**, 4281–4289.
Wollenhaupt, W. R. and Sjogren, W. L.: 1972, *The Moon* **4**, 337–347.